A New 3-D Transmission Line Matrix Scheme for the Combined Schrödinger–Maxwell Problem in the Electronic/Electromagnetic Characterization of Nanodevices

Luca Pierantoni, *Member, IEEE*, Davide Mencarelli, and Tullio Rozzi, *Life Fellow, IEEE*

***Abstract*—This paper introduces a novel technique in which Maxwell equations, discretized by the transmission line matrix method in a 3-D domain, are coupled to the Schrödinger equation and simultaneously solved. The aim is to develop a method that accounts for deterministic electromagnetic field dynamics together with the quantum phenomena, which are typical of nanodevices.**

***Index Terms*—Carbon nanotube (CNT), electromagnetic (EM) theory, Schrödinger equation, transmission line matrix (TLM).**

I. Introduction

THE CONTINUOUS growth of the telecommunication market has led to a huge demand of high-density, efficient RF, and optical systems. With the end of silicon transistor scaling perhaps in sight, carbon nanotubes (CNTs) show promise for the continued improvement of density and performance of electronic components and subsystems. Potential applications range over a wide area, including transistors [1], [2], interconnects [3], [4], nanotweezers [5], field emission devices [6], antennas [7], tunnelling structures [8], and nanowires [9]–[12] among other uses.

Despite the enormous possibilities offered by CNTs for practical applications, owing to their surprising properties as monodimensional channels, they still remain “a solution waiting for a problem.” In fact, although the above applications have been, at least partially, realized, the fabrication processes, i.e., nanotube growing and nanomanipulating, still are not mature and do not allow massive production of devices with uniform and stable characteristics.

A CNT consists of a graphene sheet (i.e., a monoatomic layer of graphite) rolled up into a cylinder, typically a few nanometers radius and length up to centimeters. Thanks to their small dimensions, nanotubes are typically defect free. Moreover, in nanotubes shorter than 70–80 nm, transport is nearly ballistic since the carriers do not couple with phonons and retain their coherence as waves. The accurate characterization of CNTs under operational conditions is a real challenge. The difficulty arises in modeling quantum phenomena coupled to Maxwell equations.

Manuscript received April 3, 2007; revised July 10, 2007.

The authors are with the Dipartimento di Elettromagnetismo e Bioingegneria, Università Politecnica delle Marche, Ancona 60100, Italy (e-mail: l.pierantoni@univpm.it; d.mencarelli@univpm.it, t.rozzi@univpm.it).

Digital Object Identifier 10.1109/TMTT.2008.916883

The transmission matrix formalism is a general technique used for the analysis of coherent transport in low-dimensional systems such as quantum wires [9] and 2-D electron gas (2DEG) confined in heterostructures. The steady-state Schrödinger equation in the frequency domain reduces to a simple wave equation, lending itself to be treated by the transmission line approach. In particular, the propagation of electrons and holes along a monodimensional system can be seen as a traveling guided-wave solution of a wave equation. It has been highlighted that interference effects may take place between co-propagating electron waves, similar to what happens for waveguide modes. Examples of these monodimensional systems are provided, besides nanotubes, by electron waveguides and nanowires. Typically, the analysis of such devices is carried out directly in the phasor domain [10]. The effects of an external electric field onto a nanodevice are computed by considering the internal dynamics of carrier transport as instantaneous with respect to the time constant of the electromagnetic (EM) transient. For example, the ac operation of nanotransistor devices has been predicted by means of a small-signal equivalent circuit, which makes use of the electrostatic limit, i.e., the solution of the Poisson–Schrödinger system. The challenge of this study is to overcome this type of simplified approach in order to develop a full-wave analysis of carrier transport, including the time transient.

Space-discretizing methods, like finite-difference time-domain (FDTD) and transmission line matrix (TLM), are well-known techniques that allow the EM full-wave modeling of 3-D structures with nearly arbitrary geometry for a wide range of applications from EM compatibility to optics [14]–[20]. As they are derived by direct discretization of Maxwell equations, they are intrinsically oriented towards solving deterministic field problems. In the literature, only very few papers have addressed the question of employing these techniques for quantum-mechanical problems. In [21], the time-dependent Schrödinger equation is solved in one dimension by the TLM. In [22], an extension of the FDTD method is applied to solve the Schrödinger equation in 3-D.

Both of the aforementioned contributions do not consider the interaction between the device and the EM field in which the structure is embedded.

The goal of this paper is to introduce a novel technique by which, for the first time, the problem is analyzed and modeled. In particular, the total EM field, including possibly an impressed

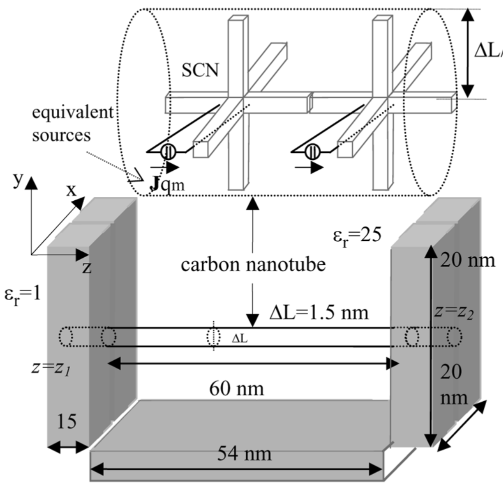

Fig. 1. Analyzed structure: two thick metallic plates (20 × 20 nm) are separated by 60 nm. A CNT is placed between the metallic electrodes.

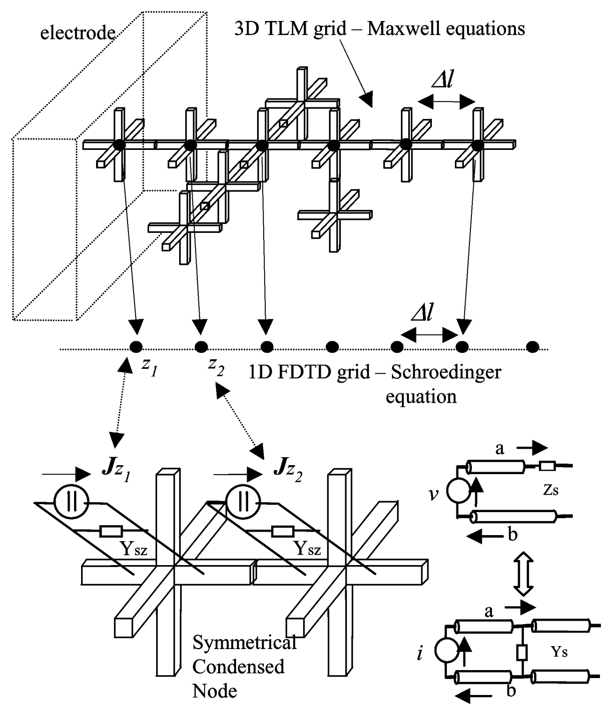

Fig. 2. Modeling of the global problem: 3-D TLM discretization and 1-D FDTD discretization. Equivalent sources and their connection to the nodes. Stub admittances of the active voltage/current sources.

external field and the self-generated EM field, arising from the macroscopic current density computed form the solution of the Schödinger equation, is consistently solved.

The proposed technique develops as follows.

1) The 3-D domain is discretized by the TLM using the symmetrical condensed node (SCN) approach.
2) Quantum phenomena are introduced in a subregion of said domain, e.g., in a 1-D chain of nodes (see Fig. 1) from one electrode ($\boldsymbol{r} = z_1$) to another ($\boldsymbol{r} = z_2$), thus simulating the presence of a nanotube.
3) At an arbitrary time step t, the EM field provides appropriate boundary conditions (source terms) for the nanotube subregion by means of the vector and scalar potentials $\boldsymbol{A}(\boldsymbol{r}, t)$ and $\phi(\boldsymbol{r}, t)$, directly calculated by the same EM field [23].
4) $\boldsymbol{A}(\boldsymbol{r}, t)$ and $\phi(\boldsymbol{r}, t)$ together with a $V_p(\boldsymbol{r})$ potential profile, which depends on the quantum properties of the nanotube and materials bounding the domain, constitute the additional terms of the Schrödinger equation [23], which is solved by means of a finite-difference scheme for that time step t. More precisely, $V_p(\boldsymbol{r})$ takes into account the static applied external field and the metal and nanotube work functions [10].
5) The wave solution $\psi(\boldsymbol{r}, t)$ generates, along the domain of the nanotube, the quantum-mechanical current $\boldsymbol{J}(\boldsymbol{r}, t)$[23], which, in turn, represents an equivalent distribution of current sources for the TLM algorithm.

These sources, located along the chain of nodes from $\boldsymbol{r} = z_1$ to $\boldsymbol{r} = z_2$, as shown in Fig. 2, affect the EM field for the next time step $t = t + \Delta t$. At that time step $t = t + \Delta t$, the TLM scheme generates a new distribution of potentials $\boldsymbol{A}(\boldsymbol{r}, t)$ and $\phi(\boldsymbol{r}, t)$ for the Schrödinger equation, and so on. This scheme is the basis of an iterative process by which the time-dependent Maxwell equations and Schrödinger equation are simultaneously solved.

In Section III, we present a first investigation of the dynamic behavior of an electron wavepacket injected in a nanotube between two metallic electrodes. The EM near field behavior is also shown.

II. Modeling Technique

A. Maxwell Equations Modeled by TLM

The TLM method introduced by Johns [15] is a space and time discretizing method of EM field computation in which the continuous space is segmented into cells by defining intersecting planes. Ports are defined at the tangential planes between two neighboring cells and a scattering center is defined at the center of each cell with the ports [15]–[18]. This physical model is called the "node" and comprises the scattering center, which is connected via transmission lines to the ports at the tangential planes between neighboring cells. Pulses are scattered at the nodes and propagate on these transmission lines to the neighboring nodes where they are scattered again. The propagation and the scattering of the wave amplitudes are expressed by operator equations [15]–[19]; the TLM is considered as the implementation of the Huygens principle [19].

The 3-D domain of the present problem (see Fig. 1) including the physical objects is modeled by means of the TLM with SCN, as in [15]–[18].

Inside the 3-D region, a 1-D chain of nodes is considered as the 1-D domain of the nanotube where the quantum dynamics is described by means of the time-domain Schrödinger equation. At each time step, the EM field is sampled along this domain, thus providing additional source terms for the Schrödinger equation, which is solved by means of a finite-difference scheme [14]. Its solution provide distributed quantum mechanical current sources, which, in turns, inject energy into the TLM nodes.

B. Schrödinger Equation

The quantum mechanical behavior of a charge carrier is described by the time-dependent Schrödinger equation

$$i\hbar\frac{\partial\psi(\mathbf{r},t)}{\partial t}=\left(-\frac{\hbar^2}{2m}\nabla^2+V(\mathbf{r})\right)\psi(\mathbf{r},t)\quad \hbar=\frac{h}{2\pi}. \quad (1)$$

The wave function $\psi(\boldsymbol{r},t)$ has no direct physical meaning, but all relevant physical parameters can be determined from it. It is complex, in fact, even though it is in the time domain. Meaningful physical quantities are determined once the complex conjugate $\psi(\boldsymbol{r},t)*$ is also employed. The basic requirement for the solutions is the following normalization condition, stating that the probability of the particle being somewhere is 1:

$$\int_{-\infty}^{+\infty}|\psi(\mathbf{r},t)|^2\,d\mathbf{r}=1. \quad (2)$$

The real function $V(\boldsymbol{r})$ is the potential, having the units of energy (eV), $h=6.26*10-34[J*s]$ is Plank's constant, m is the mass of the particle being represented by the Schrödinger equation, usually an electron, but it might be the "effective mass" of that particle in a particular semiconductor. The vector $\boldsymbol{r}=(x,y,z)$ indicates the position in a rectangular coordinates system, t is the time variable, and i is the imaginary unit.

C. Schrödinger Equation Coupled to Maxwell Equations

In the presence of an EM field, (1) is rewritten as follows [23]:

$$\left\{\frac{1}{2m}\left[\hat{\mathbf{p}}-q\mathbf{A}(\mathbf{r},t)\right]^2+q\phi(\mathbf{r},t)+V_p(\mathbf{r})\right\}\Psi(\mathbf{r},t)=i\hbar\frac{\partial\psi(\mathbf{r},t)}{\partial t} \quad (3)$$

where $A(\boldsymbol{r},t)$, $\phi(\boldsymbol{r},t)$ are vector and scalar potentials, directly related to the EM field through the appropriate gauge, e.g., the "temporal" gauge [23], and $q=-e=1.602*10-19[C]$ is the electron charge. In (3), the canonical momentum, $\boldsymbol{p}$ appears, whereas the kinematic momentum $\boldsymbol{k}$ provides the EM field contribution to the kinetic energy

$$\hat{\mathbf{p}}=-i\hbar\nabla\quad \hat{\mathbf{k}}=\hat{\mathbf{p}}-q\mathbf{A}(\mathbf{r},t). \quad (4)$$

By referring to Fig. 1, the EM field acts over a 3-D domain, whereas the Schrödinger equation describes the quantum dynamic along the 1-D domain $(z_1<z<z_2)$ where the nanotube is placed.

By taking into account the algebraic properties of operators $\boldsymbol{p}$ and $\boldsymbol{k}$, as in [23] for example, (3) becomes

$$\begin{aligned}i\hbar\frac{\partial\psi(\mathbf{r},t)}{\partial t}&=\frac{1}{2m}\left(\widehat{\mathbf{p}}^2+e\widehat{\mathbf{p}}\cdot\mathbf{A}+e\mathbf{A}\cdot\widehat{\mathbf{p}}+e^2\mathbf{A}\cdot\mathbf{A}\right)\psi(\mathbf{r},t)\\&\quad+(\phi+V(\mathbf{r}))\psi(\mathbf{r},t)\\&=\frac{1}{2m}\left\{-\hbar^2\nabla^2-ei\hbar\left[(\nabla\cdot\mathbf{A})\psi+\mathbf{A}\cdot(\nabla\psi)\right]\right.\\&\quad\left.-ei\hbar\mathbf{A}\cdot(\nabla\psi)+e^2|\mathbf{A}|^2\right\}\\&\quad+(\phi+V(\mathbf{r}))\psi(\mathbf{r},t)\\&=\frac{1}{2m}\left\{-\hbar^2\nabla^2-ei\hbar(\nabla\cdot\mathbf{A})\psi-2ei\hbar\mathbf{A}\right.\\&\quad\left.\cdot(\nabla\psi)+e^2|\mathbf{A}|^2\right\}+(\phi+V(\mathbf{r}))\psi.\end{aligned} \quad (5)$$

Now, by projecting (4) along the z-direction, we obtain

$$\begin{aligned}&\frac{1}{2m}\left\{-\hbar^2\frac{\partial^2\psi(z,t)}{\partial z^2}-2ei\hbar A_z(z,t)\right.\\&\qquad\left.\times\frac{\partial\psi(z,t)}{\partial z}-ei\hbar\psi(z,t)\frac{\partial A_z(z,t)}{\partial z}\right\}\\&\quad+(V_p(z)-e\Phi(z,t))\psi(z,t)\\&=i\hbar\frac{\partial\psi(z,t)}{\partial t}+\frac{e^2}{2m}A(z,t)^2\psi(z,t).\end{aligned} \quad (6)$$

By observing (5), we note that $A(z,t)$ and $A_z(z,t)$ are the amplitude and z-component of the potential vector $\boldsymbol{A}(\boldsymbol{r},t)$, respectively. It has been tested that the terms involving $\partial A_x/\partial x$ and $\partial A_y/\partial y$ do not provide appreciable contribution.

The $V_p(\boldsymbol{r})$ static potential profile and the $\phi(\boldsymbol{r},t)$ dynamic scalar potential are also sampled along the z-direction as $V_p(z)$ and $\phi(z,t)$, respectively.

In order to avoid complex quantities, we split (6) into two parts by separating the real and imaginary components of $\psi(\boldsymbol{r},t)$: $\psi(\boldsymbol{r},t)=\psi_R(\boldsymbol{r},t)+i\psi_I(\boldsymbol{r},t)$, i.e., $\psi(z,t)=\psi_R(z,t)+i\psi_I(z,t)$ in the z-direction. This leads to the following two coupled equations:

$$\begin{aligned}\frac{\partial\psi_R}{\partial t}&=-\frac{\hbar}{2m}\frac{\partial^2\psi_I}{\partial z^2}+\frac{1}{\hbar}\left\{\frac{e^2}{2m}A(z,t)^2-e\Phi+V_p\right\}\psi_I\\&\quad-\frac{e}{2m}\left\{2A_z\frac{\partial\psi_R}{\partial z}+\psi_R\frac{\partial A_z}{\partial z}\right\}\end{aligned} \quad (7a)$$

$$\begin{aligned}\frac{\partial\psi_I}{\partial t}&=\frac{\hbar}{2m}\frac{\partial^2\psi_R}{\partial z^2}-\frac{1}{\hbar}\left\{\frac{e^2}{2m}A(z,t)^2-e\Phi+V_p\right\}\psi_R\\&\quad-\frac{e}{2m}\left\{2A_z\frac{\partial\psi_I}{\partial z}+\psi_I\frac{\partial A_z}{\partial z}\right\}.\end{aligned} \quad (7b)$$

In a 1-D space, we approximate $\psi(z,t)$ by $\psi^n(k)=\psi(k\Delta z,n\Delta t)$, where k and n are indices and $\Delta l=\Delta z$ and Δt are the spatial and temporal steps, respectively.

Equation (7) is now discretized and solved by a finite difference-time domain scheme, as in [22], giving (8a) and (8b), shown at the bottom of the following page.

Finally, the wave function $\psi^n(k)$ of (8) is derived once an initial $\psi(\boldsymbol{z},t=0)$ distribution is defined and appropriate boundary conditions are imposed for $z=z_1z=z_2$.

D. Stability

The choices of the time step Δt and of the space-step Δl are crucial. We first choose the space-step Δl as the same for both TLM and FDTD, $\Delta l=\Delta l_{\mathrm{TLM}}=\Delta l_{\mathrm{FDTD}}$.

We then have to select Δt as the smaller value between: 1) Δt_{FDTD}, which ensures stability of the 1-D FDTD algorithm of the Schrödinger equations (5)–(8) and 2) $\Delta t_{\mathrm{TLM}} = \Delta l / H c_0$, which ensures the stability of the TLM algorithm, with c_0 being the free-space light velocity and H being the stabilization factor [15]–[21].

Concerning 1), as reported in [22], if $A(\boldsymbol{r},t) = 0$, $\phi(\boldsymbol{r},t) = 0$, Δt has to be selected so that $\Delta t \le \Delta t_{\mathrm{critical}}$ is

$$\Delta t_{\mathrm{critical}} = \frac{\hbar}{\dfrac{\hbar^2}{m\Delta z^2} + |V_p|_{\max}} \tag{9}$$

where $|V_p|_{\mathrm{MAX}}$ is the maximum absolute value of the potential $V_p(\boldsymbol{z})$ along the nanotube.

In the case of $A(\boldsymbol{r},t) \neq 0$, $\phi(\boldsymbol{r},t) \neq 0$, the spatial derivatives of $A_z(z,t)$, and the terms proportional to $|A_z(z,t)|$ give contributions that should be added in the denominator of (9).

As a matter of fact, these contributions have been tested to provide a value of $\Delta t_{\mathrm{critical}}$ an order of magnitude smaller than that of (9). In order to ensure stability, we choose a Δt_{FDTD} that is two or three orders of magnitude smaller than that of (9): $\Delta t_{\mathrm{FDTD}} \le \Delta t_{\mathrm{critical}} * 10^{-2}$.

This choice is also a constraint because we observe that, concerning 2), we always have $\Delta t_{\mathrm{TLM}} < \Delta t_{\mathrm{FDTD}}$ by some order of magnitude, thus leading to the position $\Delta t = \Delta t_{\mathrm{TLM}} = \Delta t_{\mathrm{FDTD}}$.

E. Quantum-Mechanical Current

Once (8) is solved for a time step $t = n\Delta t$, the expression of the current density is derived as in [23].

The z-component $[A]$ of such a current is

$$J_z(z,t) = q\left\{\frac{\hbar}{2im}\left(\psi^*\frac{\partial\psi}{\partial z} - \psi\frac{\partial\psi^*}{\partial z}\right) - \frac{q}{m}|\psi|^2 A_z\right\}. \tag{10}$$

The other current components are negligible due to the one-dimensionality nature of the current transport, as tested. The J_z current (10), originated by quantum mechanical phenomena, is now modeled as a $\boldsymbol{J}_d$ displacement current along the nanotube, which pumps active energy into the EM field

$$\mathbf{J}_d(\mathbf{r},t) = \frac{\partial \mathbf{D}(\mathbf{r},t)}{\partial t}. \tag{11}$$

It is noted that the above is just a working assumption *(Ansatz)* and other positions are possible. The $\boldsymbol{J}_d$ source current is sampled along the nanotube

$$\mathbf{J}_d(\mathbf{r},t) = J_z(z,t)\,\hat{\mathbf{z}} \quad J_z(z,t) = J^n(k). \tag{12}$$

Once the $J^n(k)$ distributed values of the quantum mechanical current are known, the corresponding $E_z^n(k)$ equivalent distributed voltage density sources are calculated as follows:

$$\begin{aligned} J_z(z,t) &= \varepsilon_0\varepsilon_r \frac{\partial E_z(z,t)}{\partial t} \\ \Rightarrow E_z(z,t) &= \frac{1}{\varepsilon_0\varepsilon_r}\int_0^t J_z(z,t)\,dt. \end{aligned} \tag{13}$$

These sources inject active energy into the EM field by means of the TLM chain of nodes located on the subregion zj, where $zt_1 < zj < zt_2$.

F. Modeling of the Equivalent Sources

The modeling of the equivalent TLM active sources is depicted in Fig. 2. For each node belonging to the nanotube, the local $J^n(k)$ current is equivalent to injected pulses, impinging onto the nodes and scattered from them at the next time step $t = (n+1)\Delta t$. In the model, we can refer either to equivalent current or voltage sources, depending on the chosen point of view. This conceptual equivalence is directly related to the Thevenin–Norton equivalent circuit transformation, as shown in Fig. 2, and reported as follows:

$$\begin{aligned} E_z^{n+1}(k) &= \frac{1}{\varepsilon_0\varepsilon_r(k)}\sum_{n=0}^{n} J_z^n(k)\Delta t \\ v(k) &= E_z^{n+1}(k)\,\Delta l \\ i(k) &= v(k)\,Y(k) \\ Y(k) &= Z(k)^{-1}. \end{aligned} \tag{14}$$

$$\begin{aligned} \psi_R^{n+1}(k) = \psi_R^n(k) &- \frac{\hbar}{2m}\frac{\Delta t}{(\Delta z^2)}\left\{\psi_I^{n+1/2}(k+1) - 2\psi_I^{n+1/2}(k) + \psi_I^{n+1/2}(k-1)\right\} \\ &+ \frac{\Delta t}{\hbar}\left\{\frac{e^2}{2m}\left(A^{n+1/2}(k)\right)^2 - e\phi_z^{n+1/2}(k) + V_p(k)\right\}\psi_I^{n+1/2}(k) \\ &- \frac{e\Delta t}{2m}\left\{2A_z^{n+1/2}(k)\left[\frac{\psi_R^n(k+1) - \psi_R^n(k-1)}{2\Delta z}\right] + \psi_R^n(k)\left[\frac{A_z^{n+1/2}(k+1) - A_z^{n+1/2}(k-1)}{2\Delta z}\right]\right\} \end{aligned} \tag{8a}$$

$$\begin{aligned} \psi_i^{n+1}(k) = \psi_i^n(k) &+ \frac{\hbar}{2m}\frac{\Delta t}{(\Delta z^2)}\left\{\psi_R^{n+1/2}(k+1) - 2\psi_R^{n+1/2}(k) + \psi_R^{n+1/2}(k-1)\right\} \\ &- \frac{\Delta t}{\hbar}\left\{\frac{e^2}{2m}\left(A^{n+1/2}(k)\right)^2 - e\phi_z^{n+1/2}(k) + V_p(k)\right\}\psi_R^{n+1/2}(k) \\ &- \frac{e\Delta t}{2m}\left\{2A_z^{n+1/2}(k)\left[\frac{\psi_I^n(k+1) - \psi_I^n(k-1)}{2\Delta z}\right] + \psi_I^n(k)\left[\frac{A_z^{n+1/2}(k+1) - A_z^{n+1/2}(k-1)}{2\Delta z}\right]\right\} \end{aligned} \tag{8b}$$

In (14), $Y = 1/Z = Y_{sz}$ is the Thevenin–Norton admittance/impedance, set equal to the source stub admittance/impedance, as explained below.

The technique for introducing active source elements across a set of TLM–SCN nodes has been introduced in [24], [25].

If an active device is connected to the node, the node must be consequently modified. In general, assuming that the active sources can be oriented in any one of the three orthogonal directions, three equivalent generators and three stubs with appropriate admittances must be added to the node. In the present case, the active sources and corresponding generators are z-oriented.

The scattering matrix of the new node, now taking into account the interaction between 21 lines (12 link lines and nine stubs), must be determined according to the laws of energy conservation, and assumes a form similar to that of the SCN for the modeling of electrical losses.

A full 21×21 matrix is, therefore, needed to model the material properties of the node in conjunction with the presence of the local lumped device. The coefficients of the new scattering matrix are reported in [25].

In the present case, the equivalent distributed sources are placed in the z-direction, the transverse coordinate being fixed. Taking into account the denomination of lines and ports of [18] and [20], (14) assumes the form

$$\begin{aligned} E_z^{n+1}(k) &= {}_{n+1}a^p_{\mu,x_0,y_0,k} \\ &= \frac{1}{\varepsilon_0 \varepsilon_r(x_0,y_0,k)} \sum_{n=0}^{n} J_z^n(k)\Delta t_{\mathrm{TLM}} \end{aligned} \tag{15}$$

with ${}_n a^p_{\mu,x,y,k}$ being the incident wave amplitude at the nodes (x_0, y_0, z), located at $(x_0\Delta x, y_0\Delta y, k\Delta z)$ in a Cartesian coordinate system; the p-index refers to the p-port in the SCN scattering matrix: in the present case, we have $p = 21$. The TLM grid is homogeneous with $\Delta x = \Delta y = \Delta z = \Delta L$. The μ index is set to z, where $zt_1 < z < zt_2$ is the polarization of the wave amplitude that corresponds to the local active source, as shown in Figs. 1 and 2.

In (15), the value of the ${}_{n+1}b_{\mu,x,y,k}$ reflected wave amplitude is self-consistently set to zero, as we choose the Y_{sz} source stub admittance appropriately in order to decouple the incident and reflected wave amplitudes traveling in the device stub, as reported in [24] and [25].

G. Boundary Conditions

In order to increase the accuracy, the 3-D Maxwell domain, modeled by the TLM, is bounded by the exact boundary conditions provided by the TLM–integral-equation (TLM–IE) technique [20].

For the 1-D Schrödinger domain, we impose Dirichlet boundary conditions, meaning that the wave function $\psi(\boldsymbol{z}, t)$ is set to zero at the boundaries $\psi(z_1, t) = \psi(z_2, t) = 0$ for each t.

H. Excitation

The structure can be excited: 1) by an external applied and/or impinging EM field; 2) by an initial distribution $\psi(\boldsymbol{r}, t = 0)$ wave function along the nanotube; 3) by injection of charge from the electrodes; or 4) by a combination of the above conditions. In the present work, we deal with 2).

It is noted that the problem analyzed is 1-D with respect to the Schrödinger equation, but full 3-D with respect to Maxwell equations.

III. Results

We analyze the 3-D structure of Fig. 1 having the realistic dimensions reported in the figure; the metallic electrodes present in a nanotube transistor are shown as two thick metallic plates (dimensions: 20×20 nm) separated by a distance of 60 nm. A CNT is placed between the two plates; another metallic plate, located below the CNTs, simulates a gate electrode. An insulator, of relative permittivity $\varepsilon_r = 5.7$, completely fills the space between the nanotube and gate contact.

Let us consider an electron wavepacket, previously injected inside the nanotube, whose energy is centred near the bottom of the first band of a semiconducting nanotube $(16, 0)$.

We use the index pair $(16, 0)$ defining the way the graphene sheet is rolled up (chirality). In particular, semiconducting nanotubes are those whose chirality is given by index pairs of $(n, 0)$ type. The first band is assumed to be partly occupied by electrons diffused from the lateral metallic contacts. In fact, electrons are allowed to enter the nanotube to the chosen profile of the potential $Vp(z)$ of Fig. 2, following a typical voltage bias of the electrodes [10]. We will now show the dynamic behavior of an electron wavepacket trapped inside the nanotube.

The TLM grid is homogeneous: $\Delta x = \Delta y = \Delta z = \Delta L = 1.5$ nm with $\Delta L \sim 1/10\lambda_{\mathrm{elec}}$ where $\lambda_{\mathrm{elec}} = 15.7$ nm is the electron wavelength associated to its $E_{\mathrm{elec}} = 0.1$ eV energy. The resulting grid is constituted by ($90 \times 90 \times 150$) nodes. The time step is $\Delta t = 2.5 * 10^{-3}$ fs. In the simulations we consider $n_{\mathrm{step}} = 200000$ time steps, corresponding to a time slot of $T_{\max} = 0.5$ ps.

A. Exciting Wavepacket

The exciting wavepacket $(t = 0)$ has a Gaussian spatial shape centered at $z_k = z_{kc}$. We may associate a spectral width (in energy) to the launched wavepacket by simply employing the relation between energy and wavenumber for a steady state of the Schrödinger equation (at $t = 0$, the EM field is set to zero everywhere)

$$\begin{aligned} \psi_R(z_k = k\Delta l, t = 0) &= \psi_0 \exp\left(\frac{-\left((z_k - z_{k_c})\Delta l\right)^2}{2\sigma^2}\right) \\ k_{\max} &= \frac{2\pi}{\lambda_{\mathrm{elec}}} = \left(\frac{2mE_{\mathrm{elec}}}{\hbar^2}\right)^{1/2} \\ \sigma &= \frac{\lambda_{\mathrm{elec}}}{2\pi} = \frac{1}{k_{\max}}. \end{aligned} \tag{16}$$

In (16), $\Delta k = k_{\max}$ is the width of the wavepacket in the wavenumber domain and m is the electron "effective mass" set to $0.06 * m_e$, with $m_e = 9.109 * 10^{-31}$ kg being the electron free mass [23]. The use of the effective mass approximation is consistent with the choice of such a sharp pulse (in energy). Furthermore, this choice ensures that the contribution of subbands, seen as different channels for carrier transport having

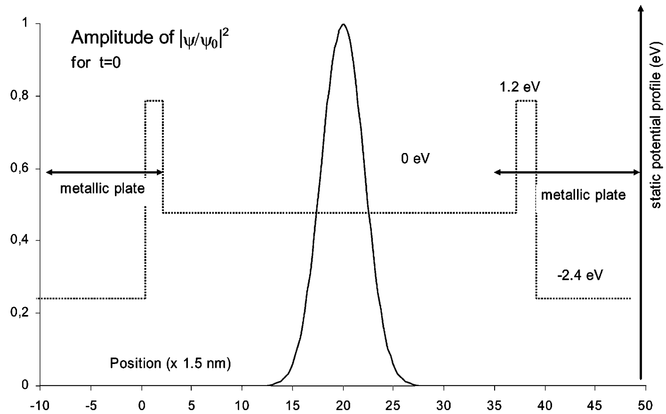

Fig. 3. Initial condition (for $t = 0$) of the incident wavepacket, centered in the middle of the nanotube and the distribution of the static potential profile.

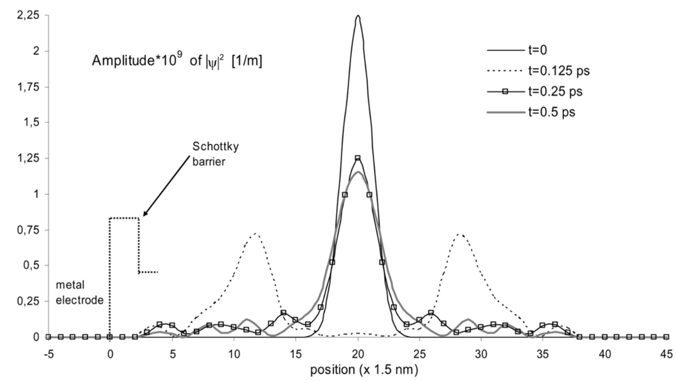

Fig. 4. Space evolution of the Gaussian wavepacket $|\psi(z,t)|^2$ for $t = 0$, $t = 0.125$, $t = 0.25$, and $t = 0.5$ ps, respectively.

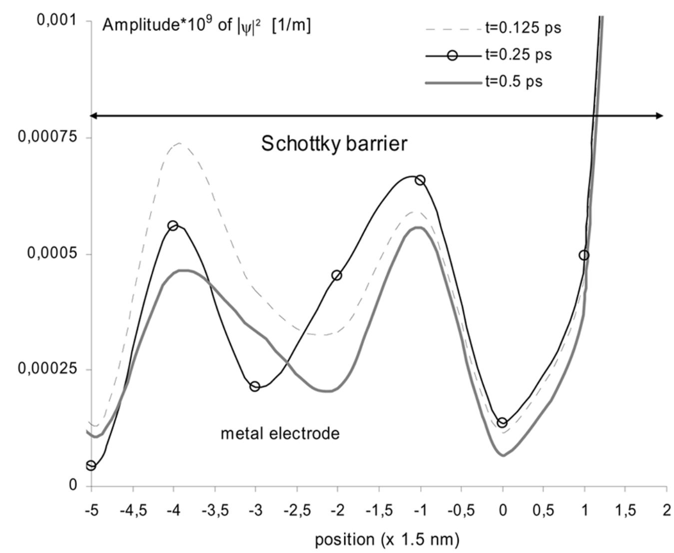

Fig. 5. Detail of the Fig. 4 penetration of the wavepacket into the potential barrier (1.2 eV) at the end of the nanotube.

different effective masses, can be neglected. No external EM field is applied at $t = 0$.

B. Injected Charge

The total charge injected in the initial $(t = 0)$ electron wavepacket is chosen according to typical values used for nanotubes embedded in a realistic device [12]. This charge is defined as the spatial integral of the linear density of charge diffused along the nanotube and depends on the operative conditions, such as: 1) the applied external voltages and 2) the geometrical parameters (electrode dimensions, nanotube size). The applied external voltages provide direct control on the electronic transmission properties of the nanotube channel. Moreover, the longer and larger the nanotube, the higher the total charge trapped between the electrodes. A typical value of the total charge for the 60-nm nanotube of Fig. 1 is estimated according to [10]. Therefore, we normalize the initial wavepacket in order to deal with a charge Q_0 that is approximately one order of magnitude greater then the electron charge $Q_0 \sim 10q$, $q = 1.602 * 10^{-19}[C]$ as follows:

$$q\int_V |\psi(\mathbf{r},0)|^2 d\mathbf{r} = q\int_{z_1}^{z_2} |\psi(z,0)|^2 dz = Q_0. \tag{17}$$

With respect to the case analyzed in [10], the Schrödinger equation (1) is solved for just one type of charge, the electron, because in the case of Fig. 1, the external bias is chosen in such a way as not to allow hole propagation. The potential profile for electrons and the initial Gaussian wavepacket are shown in Fig. 3 (the origin of the z-axis is the border of the left-side electrode): we observe the presence of Schottky barriers, detected by the electrons at the nanotube terminations.

These barriers are modeled, as a first approximation, by rectangular functions. It has to be noted that they cause the electron wavepacket to be better confined within the nanotube cavity.

The amplitude of the launched wavepacket has to be multiplied by the normalization constant of $\Psi_0(|\Psi_0|^2 \sim 1,78 * 10^9$ in the actual case), as derived from (17).

C. Wavepacket Propagation Without EM Coupling

We first analyze the case of absence of interaction between the propagating wavepacket and the EM field by setting $A_z(z,t) = \phi(z,t) = 0$ in (7) and (8).

In Fig. 4, we show the spatial evolution of the Gaussian wavepacket $|\psi(z,t)|^2$ along the nanotube domain for different time samples: for $t = 0$, $t = 0.125$, $t = 0.25$, and $t = 0.5$ ps.

It is noted that, in the described operative conditions, the wavepacket tends to be focalized after time slots of approximately $t = 0.25$ ps.

In Fig. 5, we report the detail of the wavepacket penetration through the left-side Schottky barrier (width: 3 nm). Fig. 6 gives the equivalent $\boldsymbol{J}(z,t)$ current for the same time samples of Fig. 4. In Fig. 7, we show the evolution of the Gaussian wavepacket $|\psi(z,t)|^2$ in time and space. While approaching the end of the time interval, the wavepacket $|\psi(z,t)|^2$ begins to penetrate the potential barriers, located around $z = 0$ and $z = 40$ ($\times$ 1.5 nm) in the figure.

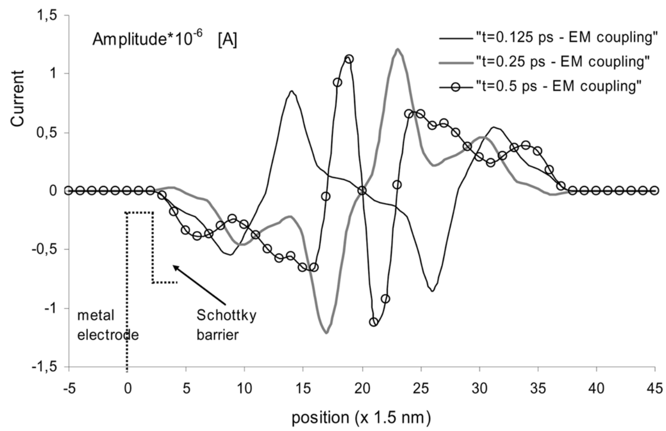

Fig. 6. Space dynamics of the current $J(z,t)$ at $t=0$, $t=0.125$, and $t=0.5$ ps, respectively.

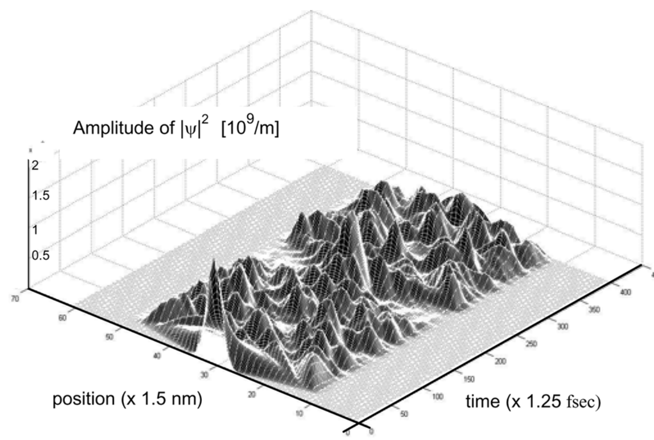

Fig. 7. Time–space evolution of the Gaussian wavepacket $|\psi(z,t)|^2$.

D. Wavepacket Propagation With EM Coupling

We now analyze the full-wave coupling between the wavepacket propagation and EM field.

In Fig. 8, we compare the spatial evolution of the Gaussian wavepacket $|\psi(z,t)|^2$ to the previous case with no EM coupling for $t=0.125$, $t=0.25$, and $t=0.5$ ps. It is remarkable to note that the EM coupling is not negligible, as it notably effects the wavepacket diffusion.

This implies that the self-induced potentials are significantly changing the "topology" of carrier transport with respect to the unperturbed case.

Fig. 9 shows the comparison of the corresponding evolution of currents for $t=0.5$ ps. Even more relevant here is the correction needed.

For a diffusion model that does not account for the EM coupling, the difference is strong, as the current contains the derivative of the electronic wave function, where we show the comparison of the corresponding evolution of currents $\boldsymbol{J}(z,t)$ for $t=0.5$ ps, highlights a remarkable relative error (the current is, in fact, related to the derivative of the wave function $\psi(z,t)$ of about 50% around the central zone.

The current density $\boldsymbol{J}(z,t)$, originated by microscopic quantum properties, can be seen as the macroscopic ballistic transport effect of the CNTs.

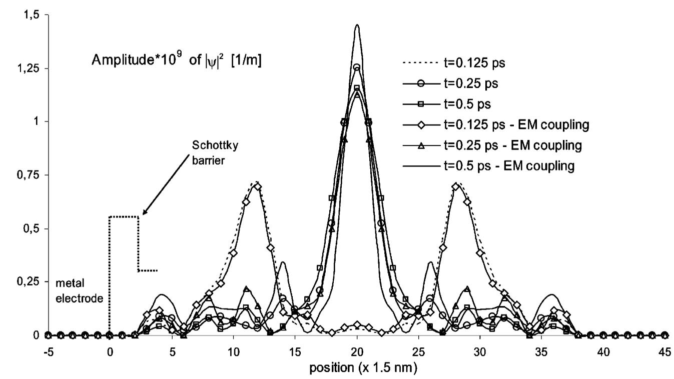

Fig. 8. Comparison between the space evolution of the Gaussian wavepacket $|\psi(z,t)|^2$ in the case of EM coupling to the case of $A_z(z,t)=\phi(z,t)=0$ for $t=0$, $t=0.125$, $t=0.25$, and $t=0,5$ ps, respectively.

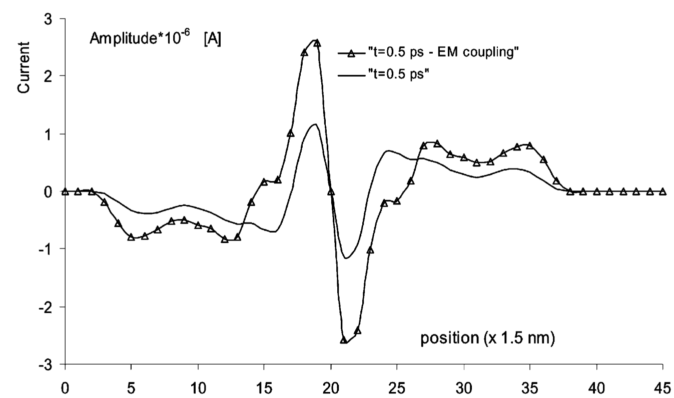

Fig. 9. Same comparison of Fig. 8, but for the quantum mechanical currents at $t=0.5$ ps.

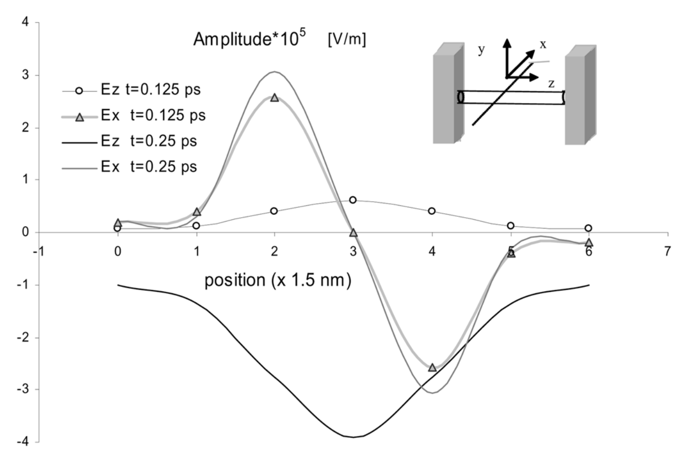

Fig. 10. Space evolution of the E_x- and E_z-field for $t=0.125$ and $t=0.25$ ps in a transversal line with respect to the nanotube.

Its characterization is the prerequisite for the calculation of the voltage–current transfer characteristics in real nanodevices, e.g., field-effect transistor devices.

In Fig. 10, we show the space evolution of the E_x- and E_z-field in a transverse domain, crossing the center of the nanotube.

It is noted that both the longitudinal E_z-field and the radial E_x-field (and E_y-field) components recall the EM field distribution related to a current traveling on a thin wire.

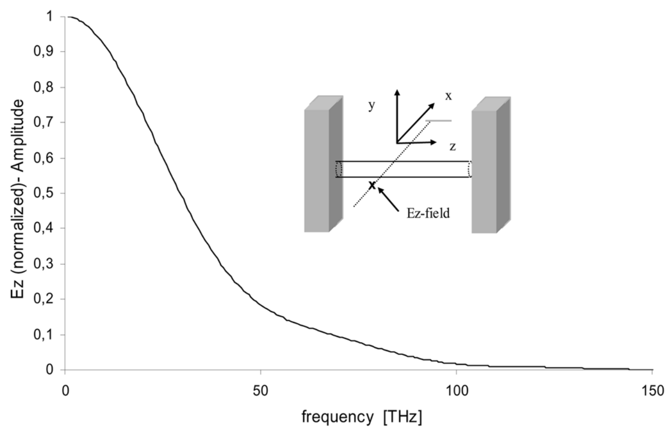

Fig. 11. Normalized spectrum of the E_z-field calculated at a point placed 3 nm close to the nanotube.

Finally, in Fig. 11, we show the frequency response (normalized amplitude) of the EM near field by sampling the E_z-field at a point placed 3 nm close to the nanotube. We observe that the spectrum extends up to frequencies corresponding to $\lambda = c/f$ optical wavelengths with $c = c_o\varepsilon_r^{-1/2}$ and $\varepsilon_r = 5.7$.

IV. Conclusions

The goal of this study was to build a TLM scheme capable of dealing with newly emergent structures based on quantum transistor devices such as nanotube transistors. For this purpose, we have introduced a novel numerical technique in which Maxwell equations are coupled to the Schrödinger equation and solved self-consistently.

A first application of the method to the injection of charge into the nanotube has shown the TLM scheme capable of describing the resulting EM transient. Possible applications are in the simulation of high-frequency nanotransistor and nano-light-emitting diodes (LEDs).

References

[1] S. Li, Z. Yu, S. F. Yen, W. C. Tang, and P. J. Burke, “Carbon nanotube transistor operation at 2.6 GHz,” *Nano Lett.*, vol. 4, pp. 753–756, 2004.

[2] J. P. Clifford, D. L. John, L. C. Castro, and D. L. Pulfrey, “Electrostatics of partially gated carbon nanotube FETs,” *IEEE Trans. Nanotechnol.*, vol. 3, no. 2, pp. 281–286, Jun. 2004.

[3] P. J. Burke, “Lüttinger liquid theory as a model of the GHz electrical properties of CNs,” *IEEE Trans. Nanotechnol.*, vol. 1, no. 3, pp. 129–144, Sep. 2002.

[4] P. J. Burke, “An RF circuit model for CNs,” *IEEE Trans. Nanotechnol.*, vol. 2, no. 1, pp. 55–58, Mar. 2003.

[5] P. Kim and C. M. Lieber, “Nanotube nanotweezers,” *Science*, vol. 286, pp. 2148–2150, 1999.

[6] G. Pirio, P. Legagneux, D. Pribat, K. B. K. Teo, M. Chhowalla, G. A. J. Amaratunga, and W. I. Milne, “Fabrication and electrical characteristics of carbon nanotube field emission microcathodes with an integrated gate electrode,” *Nanotechnology*, vol. 13, pp. 1–4, Feb. 2002.

[7] G. W. Hanson, “Current on an infinitely long carbon nanotube antenna excited by a gap generator,” *IEEE Trans. Microw. Theory Tech.*, vol. 54, no. 1, pp. 76–81, Jan. 2006.

[8] H. Sanada, M. Suzuki, and N. Nagai, “Analysis of resonant tunneling using the equivalent transmission-line model,” *IEEE Trans. Quantum Electron.*, vol. 33, no. 5, pp. 731–741, May 1997.

[9] A. V. Maslov and C. Z. Ning, “Modal gain in a semiconductor nanowire laser with anisotropic bandstructure,” *IEEE J. Quantum Electron.*, vol. 40, no. 10, pp. 1389–1397, Oct. 2004.

[10] T. Rozzi, D. Mencarelli, A. Di Donato, and M. Farina, “Self-consistent analysis of carbon nanotube (CNT) transistors: State-of-the-art and critical discussion,” in *Proc. 7th Int. RF MEMs and RF Microsyst. Conf.*, Orvieto, Italy, Jun. 2006, pp. 59–61.

[11] D. Mencarelli, T. Rozzi, L. Maccari, A. D. Donato, and M. Farina, “Electronic properties of carbon nanotubes investigated by means of standard electromagnetic simulators,” *Phys. Rev.*, vol. B 75, 2007, 085402.

[12] M. Pourfath, H. Kosina, B. H. Cheong, W. J. Park, and S. Selberherr, “The effect of device geometry on the static and dynamic response of carbon nanotube field effect transistors,” in *Proc. 5th Nanotechnol. Conf.*, 2005, pp. 758–761.

[13] P. L. McEuen, M. S. Fuhrer, and H. Park, “Single-walled carbon nanotube electronics,” *IEEE Trans. Nanotechnol.*, vol. 1, no. 1, pp. 78–85, Mar. 2002.

[14] A. Taflove, *Computational Electrodynamics—The Finite-Difference Time-Domain Method*. Boston, MA: Artech House, 1995.

[15] P. B. Johns, “A symmetrical condensed node for the TLM method,” *IEEE Trans. Microw. Theory Tech.*, vol. MTT-35, no. 4, pp. 370–377, Apr. 1987.

[16] H. Jin and R. Vahldieck, “Direct derivation of TLM symmetrical condensed node and hybrid symmetrical condensed node from Maxwell’s equations using centered differencing and averaging,” *IEEE Trans. Microw. Theory Tech.*, vol. 42, no. 12, pp. 2554–2562, Dec. 1994.

[17] V. Trenkic, C. Christopoulus, and T. M. Benson, “Optimization of TLM schemes based on the general symmetrical condensed node,” *IEEE Trans. Antennas Propag.*, vol. 45, no. 3, pp. 457–465, Mar. 1997.

[18] M. Krumpholz and P. Russer, “A field theoretical derivation of TLM,” *IEEE Trans. Microw. Theory Tech.*, vol. 42, no. 9, pp. 1660–1668, Sep. 1994.

[19] W. J. R. Hoefer, “The transmission-line-matrix method—Theory and applications,” *IEEE Trans. Microw. Theory Tech.*, vol. MTT-35, no. 10, pp. 882–893, Oct. 1985.

[20] L. Pierantoni, A. Massaro, and T. Rozzi, “Accurate modeling of TE/TM propagation and losses of integrated optical waveguide,” *IEEE Trans. Microw. Theory Tech.*, vol. 53, no. 6, pp. 1856–1862, Jun. 2005.

[21] P. Enders and D. D. Cogan, “TLM routines for the paraxial wave equation and the time-dependent Schrödinger equation,” in *Proc. 1st Int. Transmission Line Matrix Modeling Workshop*, Victoria, BC, Canada, Aug. 1–3, 1995, pp. 137–140.

[22] A. Soriano, E. A. Navarro, J. A. Portì, and V. Such, “Analysis of the finite difference time domain technique to solve the Schrödinger equation for quantum devices,” *J. Appl. Phys.*, vol. 95, no. 12, pp. 8011–829, Jun. 2004.

[23] J. H. Davis, *The Physics of Low-Dimensional Semiconductor*. Cambridge, U.K.: Cambridge Univ. Press, 1998.

[24] P. Russer, W. J. R. Hoefer, and P. P. M. So, “Modeling of nonlinear active regions in TLM,” *IEEE Microw. Guided Lett.*, vol. 1, no. 1, pp. 10–13, Jan. 1991.

[25] L. Cascio and W. J. R. Hoefer, “Modification of the 3D-TLM scattering matrix to model nonlinear devices in graded and heterogeneous regions,” in *IEEE MTT-S Int. Microw. Symp. Dig.*, Jun. 7–12, 1998, vol. 2, pp. 897–900.

Luca Pierantoni (M’94) was born in Maiolati Spontini, Italy, in 1962. He received the Laurea (*summa cum laude*) degree in electronics engineering and Ph.D. degree from the University of Ancona, Ancona, Italy, in 1988 and 1993, respectively.

From 1989 to 1995, he was a Research Fellow with the Department of Electronics and Automatics, University of Ancona. From 1996 to 1998, he was a Senior Research Scientist with the Institute of High-Frequency Engineering, Technical University of Munich, Munich, Germany. In 1999, he joined the Dipartimento di Elettromagnetismo e Bioingegneria, Università Politecnica delle Marche, Ancona, Italy, as an Assistant Professor. His current research interests are the development of analytical/numerical methods for the modeling of integrated optical circuits and nanodevices.

Dr. Pierantoni has been a member of the Italian National Institute for the Physics of Matter (INFM) since 2001.

Davide Mencarelli received the Laurea degree (*summa cum laude*) in electronics engineering from the Università Politecnica delle Marche, Ancona, Italy, in 2002, and is currently working toward the Ph.D. degree in electromagnetics at the Università Politecnica delle Marche.

He is currently with the Dipartimento di Elettromagnetismo e Bioingegneria, Università Politecnica delle Marche. His research interests are the analysis and modeling of integrated optical devices. He is currently involved with nonlinear electrooptic materials and periodic photonic structures.

Mr. Mencarelli has been a member of the Italian National Institute for the Physics of Matter (INFM) since 2007.

Tullio Rozzi (M'66–SM'74–F'90–LF'07) received the Dottore degree in physics from the University of Pisa, Pisa, Italy, in 1965, the Ph.D. degree in electronic engineering from The University of Leeds, Leeds, U.K., in 1968, and the D.Sc. degree from the University of Bath, Bath, U.K., in 1987.

From 1968 to 1978, he was a Research Scientist with the Philips Research Laboratories, Eindhoven, The Netherlands. In 1975, he spent one year with the Antenna Laboratory, University of Illinois at Urbana-Champaign. In 1978, he became the Chair of Electrical Engineering with the University of Liverpool. In 1981, he became the Chair of Electronics and Head of the Electronics Group, University of Bath, where he was also Head of the School of Electrical Engineering on an alternate three-year basis. Since 1988, he has been a Professor with the Dipartimento di Elettromagnetismo e Bioingegneria, Università Politecnica delle Marche, Ancona, Italy, where he is also Head of the department.

Dr. Rozzi was the recipient of the 1975 Microwave Prize presented by the IEEE Microwave Theory and Technique Society (IEEE MTT-S). He has been a member of the Italian National Institute for the Physics of Matter (INFM) since 2001.